Journal Name

ARTICLE TYPE

Cite this: DOI: 00.0000/xxxxxxxxxx

Vapour-liquid phase equilibria and interfacial properties of fatty acid methyl esters from molecular dynamics simulations

Esther Feria,[a] Jesús Algaba,[a] José Manuel Míguez,[a] Andrés Mejía,[b] Paula Gómez-Álvarez,[a] and Felipe J. Blas,*[a]

Received Date
Accepted Date

DOI: 00.0000/xxxxxxxxxx

We have determined the phase equilibria and interfacial properties of methyl esters homologous series (from methyl acetate to methyl heptanoate) from direct simulation of the vapour-liquid interface. Methyl esters are modelled using the united atom approach in combination with the TraPPE force fields for alkanes, alkenes, carbon dioxide, ethers, and carboxylic acids in a transferable way. This allows to take into account explicitly both dispersive and coulombic interactions, as well as the repulsive Pauli-exclusion interactions. Simulations are performed in the NVT or canonical ensemble using molecular dynamics. Vapour-liquid surface tension is determined using the virial route, i.e., evaluating the normal and tangential components of the pressure tensor along the simulation box. We have also calculated density profiles, coexistence densities, vapour pressures, surface entropies and enthalpies, and interfacial thickness as functions of temperature, as well as the normal boiling temperatures and the critical temperatures, densities, and pressures for each member of the series. Special attention is paid to the comparison between experimental data taken from the literature and our results obtained from molecular dynamic simulations. We also analyze the effect of increasing the molecular weight of the methyl esters (at fixed temperature) on all the properties considered, with special emphasis on phase equilibria envelopes and surface tension. The TraPPE force fields transferred from other molecules and chemical families are able to predict very accurately the experimental vapour-liquid phase envelopes of methyl esters. We also compare the results obtained from simulations for the surface tension with experimental data taken from the literature. To our knowledge, this is the first time that vapour-liquid phase equilibria and interfacial properties, and particularly surface tension, of the methyl esters homologous series are obtained from computer simulation.

1 Introduction

Current environmental regulations and energy directives recommend and promote to increase, at least 10%, the use of renewable fuels for transport by 2020, and also to dramatically reduce the transportation emission levels by 2030[1]. These initiatives have been motivated to reduce greenhouse gas emissions, where transportation contributes 34% of the total emissions. One of the most groundbreaking alternatives to accomplish these targets is to replace (partially or totally) the fossil-fuels based by biofuels (fuels produced from natural renewable sources), where one of the most recently emerging biofuels is the biodiesel. Biodiesel are considered the third (or fourth) generation of biofuels[2] due to they are renewable, biodegradable, non-toxic, produces less carbon dioxide than fossil fuels, and also they can replace the petroleum diesel and be used either in their neat form or blended with fossil diesel inside of the compression ignition engines without any extensive engine modification. In general terms, biodiesel can be obtained from a group of mono-alkyl esters[3] that, depending on the alcohol (methanol or ethanol) used for the transesterification process, become Fatty Acid Methyl Esters (FAMEs) or Fatty Acid Ethyl Esters (FAEEs), respectively. From a technical viewpoint, the use of FAMEs as a fuel is more developed than FAEEs[4,5] for efficient use.

Despite the novel use of FAMEs as diesel fuel, systematic research concerning the characterization of interfacial properties

[a] Laboratorio de Simulación Molecular y Química Computacional, CIQSO-Centro de Investigación en Química Sostenible and Departamento de Ciencias Integradas, Universidad de Huelva, 21007 Huelva, Spain.
[b] Departamento de Ingeniería Química, Universidad de Concepción, POB 160-C Concepción, Chile.
* Corresponding author, e-mail: felipe@uhu.es

(*e.g.*, the interfacial concentration of species, the interfacial thickness, the superficial enthalpy and entropy, and surface or interfacial tension) of pure and mixtures with FAMEs is very limited. For the case of pure short chain FAMEs (*i.e.*, from methyl acetate to methyl heptanoate), the available experimental data for interfacial tensions reported in DECHEMA[6] and Landolt-Börnstein[7–9] databases and also the DIRPP[10] and NIST correlations[11], only cover a narrow temperature range (273 K to 360 K). Theoretical models, such as the Square Gradient Theory[12], need the experimental data of interfacial tensions to fit their parameters and use them as a model to predict the other interfacial properties. For the case of mixtures, the scenario is even worse, especially for the case of mixtures of hydrocarbons or aromatics with FAMEs, where interfacial properties are unexplored and only very few sparse data can be found. The only exception is the case of water + FAMEs mixtures, where both experimental determinations and theoretical modeling have been carried out by one of us.[13] Therefore, considering the environmental regulations and energy directives, it is necessary to carry out systematically exploration of the interfacial behavior of the compounds involved in the biodiesel production. These properties are the key requirement for their future use as a fuel, as well as for environmental issues, such as the removal of contaminants from water and for groundwater remediation[14,15]. Consequently, this work has focused on the determination of some selected interfacial properties for the case of pure short-chain FAMEs from methyl acetate to methyl heptanoate.

Due to the lack of predictive theories, molecular dynamics (MD) simulations can be used as a predictive tools to explore both bulk properties (*i.e.*, coexistence density curve, $T-\rho$, vapour pressure or Clapeyron curve, $P-T$) and interfacial properties (*e.g.*, interfacial concentration of species, the interfacial thickness, the superficial enthalpy and entropy, and surface or interfacial tension) from low temperature to near the critical point.

In the last decades, computer simulation has become an essential tool for modelling and predicting thermodynamic properties, including phase equilibria and interfacial properties, of complex systems of fundamental and applied interest. In particular, during the last twenty years, a remarkable progress has been made in the development of new force fields for describing complex molecules from a molecular perspective. Perhaps, the most relevant example of this kind of force fields is the transferable parameters for phase equilibria (TraPPE) approach of Siepmann and coworkers[16], that allows to determine with high accuracy thermodynamic and structural properties of complex molecules. The key idea behind the TraPPE models is transferability, i.e., to predict the behaviour of a given molecule or set of molecules only from the knowledge of molecular parameters for particular chemical groups taken unchanged from other systems, regardless of the atomic makeup of the rest of the molecule. This strategy allows to truly predict the thermodynamic and other structural and dynamical properties without the need of adjustments to experimental data of the system under study.

In work, we use the united-atoms (UA) version of the Transferable Parameters for Phase Equilibria approach (TraPPE-UA) to predict the phase behaviour and interfacial properties of FAMEs. As it is mentioned in the previous paragraph, it would be possible to obtain new molecular parameter values according to the TraPPE-UA force fields by fitting to experimental vapour-liquid phase equilibria. However, following Kamath *et al.*[17], it is also possible to use the parameter values from the TraPPE-UA database for chemical groups that describe different molecules, including alkane and alkenes, carbon dioxide, ethers, and carboxylic acids, and transfer them to predict the phase equilibria and interfacial properties of the first members of the methyl esters chemical family. The main goal of this work is to use the transferable molecular parameters of the TraPPE-UA force field to predict the phase equilibria and interfacial properties of the first members of linear methyl esters using MD simulation. In particular, we use the direct coexistence technique in the NVT or canonical ensemble. The results obtained from MD simulation are with experimental data taken from the literature[11] to critically assess the models ability. To our knowledge, this is the first time that the vapour-liquid interfacial properties, and particularly the surface tension, of the first members of the methyl esters chemical family are determined from computer simulations.

The organization of this paper starts with the description of molecular models in Section 2. In the next section, Section 3, simulation details are provided and explained briefly. In Section 4, the main results of interfacial properties are presented and discussed. Finally, the main conclusions are summarized in the last section.

2 Molecular models

As we have mentioned, methyl esters have been modeled following the united-atom approach. In all cases, the force fields use the Lennard-Jones and Coulomb potentials to describe the non-bonded interactions,

$$U(r_{ij}) = 4\varepsilon_{ij}\left[\left(\frac{\sigma_{ij}}{r_{ij}}\right)^{12} - \left(\frac{\sigma_{ij}}{r_{ij}}\right)^{6}\right] + \frac{q_i q_j}{4\pi\varepsilon_0 r_{ij}} \qquad (1)$$

where r_{ij} is the distance between interacting sites i and j, σ_{ij} and ε_{ij} are the diameter and well depth associated to the LJ intermolecular potential, q_i and q_j are the partial charges on interacting sites i and j, and ε_0 the permittivity of vacuum. All the LJ parameters for unlike interactions are obtained using the Lorentz-Berthelot combining rules.

According to the TraPPE-UA philosophy, molecular parameters are taken from existing parametrizations and combined to form the molecules of interest, as it has been explained in the previous section. Molecular parameters for non-bonded interactions for the carbonyl chemical group (C=O) are taken from molecular parameters of two different molecules: The parameters of the carbonyl oxygen are taken from the oxygen parameters of the carbon dioxide model proposed by Potoff and Siepmann[18], and the parameters of the carbonyl carbon are taken from the carbon parameters of the carboxylic acids models proposed by Kamath *et al.*[19]. The molecular parameters involved in the methoxy (or terminal methyl group bonded to the ether oxygen, –O–CH_3), i.e., the ether oxygen and the methyl group CH_3 (sp^2), are taken from

Table 1 Well depth, ε, size, σ, and partial charges, q, parameters for the TraPPE-UA force field corresponding to non-bonded interactions of methyl-esters (from methyl acetate to methyl heptanoate). Letters in parentheses indicate the atom a particular sites is bonded to. All values are taken from the works of Siepmann and co-workers [18–21]. See also the TraPPE webpage [16].

Atom	ε/k_B(K)	σ(Å)	q(e)
$\mathbf{CH_3}-(\mathrm{O})$	98.0	3.75	0.25
$-\mathbf{O}-$	55.0	2.80	-0.40
$\mathbf{C}=(\mathrm{O})$	41.0	3.90	0.55
$\mathbf{O}=(\mathrm{C})$	79.0	3.05	-0.45
$\mathbf{CH_3}-(\mathrm{C})$	98.0	3.75	0.05
$\mathbf{CH_2}-(\mathrm{C})$	46.0	3.95	0.05
$\mathbf{CH_3}-(\mathrm{CH}_x)$	98.0	3.75	0.00
$\mathbf{CH_2}-(\mathrm{CH}_x)$	46.0	3.95	0.00

the work of Stubbs *et al.* [20] The molecular parameters of methyl (CH_3– not bonded to the oxygen ether) and methylene (–CH_2– not bonded to the carbon –C– atom) groups are taken from the TraPPE-UA parameter values of alkanes proposed by Martin and Siepmann [21]. It is interesting to mention that Maerzke *et al.* [22] considered TraPPE force field for acrylates and metacrylates that share some of the same united atoms as the FAMEs studied in this work. However, these substances contain conjugated double bonds. In our work, we consider methyl esters that do not contain this kind of bonds, and due to that to use the TraPPE molecular parameters of Kamath *et al.* [19] and Stubbs *et al.* [20]. All the molecular parameters used in this work to describe the non-bonded interactions, including the partial charges values for electrostatic interactions of all the chemical groups, are summarized in Table 1.

Table 2 Bond length values for the TraPPE-UA force field corresponding to methyl-esters (from methyl acetate to methyl heptanoate). All values are taken from the TraPPE webpage [16].

Bond	Bond length (Å)
C = O	1.200
C – O	1.344
CH_3 – O	1.410
CH_x – C	1.520
CH_2 – CH_x	1.540

As in the case of the LJ parameters and partial charges, bond lengths, bending, and torsional force field parameters characterizing the bonded interactions are obtained from the TraPPE-UA values of different chemical groups. Tables 2, 3, and 4 collect all the parameter values used in this work. Note that according the usual TraPPE-UA force field approach, the bond length between different chemical groups are fixed.

3 Simulation details

All MD simulations are carried out in conditions at which the vapour-liquid interface is present, following the standard methodology [23,24] for all models studied. In particular, simulations are performed in the NVT canonical ensemble using GROMACS (version 4.6.1) [25] at a fixed temperature T, in a parallelepipedic simulation cell of constant volume $V = L_x \times L_y \times L_z$, where L_x, L_y, and L_z are the dimensions of the simulation box. We use periodic boundary conditions in all three directions.

Table 3 Bending potential parameters for the TraPPE-UA force field corresponding to methyl-esters (from methyl acetate to methyl heptanoate). All values are taken from the TraPPE webpage [16].

Bending	θ (deg)	k_θ/k_B (K/rad^2)
CH_3–O–C	115	62500
O–C=O	125	62500
O–C–CH_3	110	70596
O=C–CH_3	125	62500
O=C–CH_2	125	62500
C–CH_2–CH_2	114	62500
CH_2–CH_2–CH_2	114	62500
CH_2–CH_2–CH_3	114	62500

A homogeneous liquid system is first equilibrated in a parallelepiped simulation box. The dimensions of the box are $L_x = L_y = 3.9$ nm for the case of methyl acetate and $L_x = L_y = 3.95$ nm for the rest of methyl esters. For the lengths of the simulation boxes along the z-axis we have used the following sizes: $L_z = 11$ nm (methyl acetate), $L_z = 13$ nm (methyl propionate), $L_z = 16$ nm (methyl butyrate), $L_z = 19$ nm (methyl valerate), $L_z = 20$ nm (methyl hexanoate), and $L_z = 23$ nm (methyl heptanoate). We consider $N = 1100$ molecules for all the methyl esters studied in this work. After equilibration of these bulk-liquid systems, the box is expanded along the z direction leaving the liquid phase slab at the center. The final overall dimensions of the vapour-liquid-vapour configuration box are therefore $L_x = L_y = 3.9$ nm and $L_z = 33$ nm for the case of methyl acetate, and $L_x = L_y = 3.95$ nm and $L_z = 39$, 48, 57, 60, and 69 nm for the methyl propionate, methyl butyrate, methyl valerate, methyl hexanoate, and methyl heptanoate, respectively.

In order to reduce the truncation and system size effects involved in the phase equilibrium and interfacial properties calculations, the cut-off radius (r_c) has been taken equal to a value of 5σ ($r_c = 1.95$ nm for methyl acetate and 1.975 nm for the rest of methyl esters). It has been shown by several authors [26–28] that such a value provides a reasonable description for the interfacial properties. Long-range interactions are determined using three-dimensional Ewald technique with a convergence parameter of 0.1 Å^{-1} and a maximum value for the reciprocal lattice equal to 31 is used.

We have used the Verlet leapfrog [29] algorithm with a time step of 0.001 ps. It is important to note in this case that the time step value chosen has been necessary to sample correctly the torsional potentials of esters models. A Nosé-Hoover thermostat [30] with large time constant equal to 1.0 ps has been used. Simulations of the homogeneous liquid systems are equilibrated during 5 ns. After this, the vapour-liquid-vapour systems are also equilibrated during 5 ns. After the systems reach equilibrium, the properties of the coexisting vapour and liquid phases are obtained as appropriate averages during 20 ns. In order to estimate errors on the variables computed, the sub-blocks average method has been applied. [31] In such approach, the production period is divided into M independent blocks. The statistical error is then deduced from the standard deviation of the average $\bar{\sigma}/\sqrt{M}$, where $\bar{\sigma}$ is the variance of the block averages and M has been fixed in this work to $M = 10$.

The equilibrium vapour pressure, P, and interfacial tension, γ,

Table 4 Torsional potential parameters for the TraPPE-UA force field corresponding to methyl-esters (from methyl acetate to methyl heptanoate). All values are taken from the TraPPE webpage [16].

Torsion	c_0/k_B (K)	c_1/k_B (K)	c_2/k_B (K)	c_3/k_B (K)
CH_3–O–C=O	11594.6	3374.2	-4118	-613.6
CH_3–O–C–CH_3	6551.3	1566.1	-4196	789.2
CH_3–O–C–CH_2	6551.3	1566.1	-4196	789.2
O–C–CH_2–CH_2	839.87	-2133.17	106.68	3097.72
O–C–CH_2–CH_3	839.87	-2133.17	106.68	3097.72
O=C–CH_2–CH_2	1121.13	142.79	-115.68	-1172.92
O=C–CH_2–CH_3	1121.13	142.79	-115.68	-1172.92
C–CH_2–CH_2–CH_2	1009.97	-2018.93	136.38	3165.28
C–CH_2–CH_2–CH_3	1009.97	-2018.93	136.38	3165.28
CH_2–CH_2–CH_2–CH_2	1009.97	-2018.93	136.38	3165.28
CH_2–CH_2–CH_2–CH_3	1009.97	-2018.93	136.38	3165.28

are obtained from the diagonal components of the pressure tensor. The vapour pressure corresponds to the normal component, $P \equiv P_{zz}$, of the pressure tensor, while the interfacial tension is obtained using the mechanical route [32–35] as:

$$\gamma = \frac{L_z}{2}\left[P_{zz}(z) - \frac{P_{xx}(z)+P_{yy}(z)}{2}\right] \tag{2}$$

In Eq. (2), the additional factor $1/2$ comes from having two interfaces in the system, and L_z is the size of the simulation box in the z direction, defined along the longitudinal dimension across the interface.

The experimental determination of the critical state of FAMEs is extremely difficult due to their thermal instability. One alternative route to obtain the critical coordinates, i.e., critical pressure, P_c, temperature, T_c, and density, ρ_c, is to use the vapour-liquid equilibrium MD results together the scaling law [36,37] given by:

$$\rho_L - \rho_V = A(T - T_c)^{\beta} \tag{3}$$

and the corresponding law of rectilinear diameters

$$\frac{\rho_L + \rho_V}{2} = \rho_c + B(T - T_c) \tag{4}$$

β is the corresponding critical exponent [33], with a universal value of $\beta = 0.325$, and A, B, T_c and ρ_c are four unknown constants obtained fitting to the simulation results. ρ_L and ρ_V are the liquid and vapour coexistence densities at the corresponding temperature T, respectively. Critical temperature, T_c, and density, ρ_c, can be easily obtained from Eqs. (3) and (4).

An independent way to calculate T_c is to apply an alternative scaling law using interfacial information from the system. [38,39] Following this route, γ is related to T_c by the following expression:

$$\gamma = \gamma_0 (1 - T/T_c)^{\mu} \tag{5}$$

where γ_0 is the so-called "zero-temperature" surface tension and μ is the corresponding critical exponent. Here, we fix μ to the universal value $\mu = 1.258$ as obtained from renormalization-group theory. [33] Once again, the unknown constants, γ_0 and T_c are found by fitting the interfacial tension data with temperature.

The critical pressure can be estimated from an extrapolation of the Clausius-Clapeyron relation to the critical temperature obtained from Eq. (3) or Eq. (5):

$$\ln P = C_1 + \frac{C_2}{T} \tag{6}$$

where C_1, and C_2 are correlation parameters. The value of P_c is obtained using Eq. (6) at $T = T_c$. The critical temperature value, T_c, used in the previous equation is obtained from Eq. (3).

The surface entropy (Δs^{γ}) and surface enthalpy (Δh^{γ}) change of surface formation can be also determined using the temperature dependence of the surface tension from the following derivative expressions [33,40]:

$$\Delta s^{\gamma} = -\left(\frac{\partial \gamma}{\partial T}\right)_P \tag{7}$$

$$\Delta h^{\gamma} = \gamma + T\Delta s^{\gamma} \tag{8}$$

Finally, an interesting property that can be obtained from the calculation of density profiles is the interfacial width along the vapour-liquid equilibrium. Implicitly this property is defined by fitting the curves from the original mean field van der Waals theory, [33] described by

$$\rho(z) = \frac{\rho_L + \rho_V}{2} - \frac{\rho_L - \rho_V}{2}\tanh\left[\frac{\alpha(z - z_0)}{d}\right] \tag{9}$$

where the constant $\alpha = 2\tanh^{-1}(0.8)$ is chosen so that d is the 10-90 interfacial thickness and z_0 the position of the Gibbs dividing surface. If coexistence densities are calculated previously (see the next section for further details), d and z_0 could be treated as adjustable parameters in Eq. (9). Since two interfaces are simulated simultaneously during each simulation, it is possible to compare the interfacial thickness values obtained from both interfaces. In this work, the values determined are always found to be the same within statistical uncertainty, indicating that the inhomogeneous systems are properly equilibrated at all temperatures.

4 Results and discussion

In this section we present the main results from the simulations of the six methyl esters using the TraPPE-UA molecular models described in the previous sections. We focus on the interfacial properties, such as density profiles, interfacial thickness, surface entropy and enthalpy, and surface tension. We also examine the temperature dependence of these properties, and compare our results for the different models with experimental data taken from the literature [11].

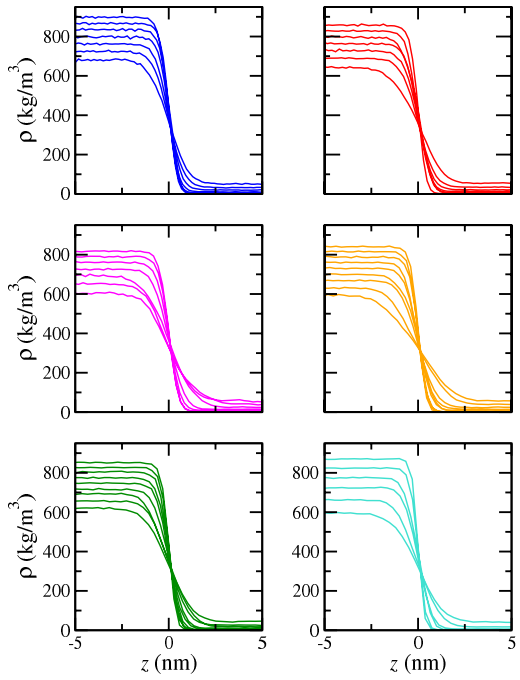

Fig. 1 Simulated equilibrium density profiles across the vapour-liquid interface of methyl esters as obtained from MD NVT simulations using the TraPPE -UA models for (a) methyl acetate (blue curves), (b) methyl propionate (red curves), (c) methyl butyrate (magenta curves), (d) methyl pentanoate (orange curves), (e) methyl hexanoate (green curves), and (f) methyl heptanoate (turquoise curves) at different temperatures. From bottom to top (in the liquid region): 300, 325, 350, 375, 400, 425, 450, 475, 500, 525, and 550 K

We analyze the thermodynamic and interfacial behavior of all the FAMEs at different temperatures using the same methodology that in our previous works.[41–47] Density profiles are calculated by dividing the system in 200 slabs along the z direction. The molecular density profiles, $\rho_i(z)$, are obtained by assigning the position of each united atom center, z_i, to the corresponding slab and constructing the molecular density from mass balance considerations. The bulk vapour and liquid densities in each system are calculated by averaging $\rho_i(z)$ over appropriate regions sufficiently removed from the interfacial region. In addition to that, the final bulk vapour density value, at each temperature and chain length, is obtained after averaging the density profiles on both sides of the liquid film.

We show in Fig. 1 the density profiles $\rho(z)$ for the six methyl esters considered in this work, from methyl acetate up to methyl heptanoate, at different temperatures as modelled using the TraPPE-UA models. For the sake of clarity, we only present one half of the profiles corresponding to one of the interfaces. Also for convenience, all density profiles have been shifted to place z_0 at the origin.

As can be seen, liquid density decreases and vapour density increases as the temperature is increased in all cases as expected. The slope of each density profile, in absolute value, along the interfacial region becomes smaller as the temperature approaches the critical point for each system. According to the near-critical scaling laws[33], the interfacial thickness must diverge as the temperature approaches the critical temperature. The results presented in Fig. 1 corroborate this behaviour.

From the density profiles depicted in the previous Figure, it is possible to obtain the vapour-liquid phase envelopes of the different FAMEs studied in this work. Results corresponding to the vapour and liquid coexistence densities, at different temperatures, are presented in Table 5. Fig. 2 shows the phase diagrams of all the systems considered as obtained from MD computer simulations. Experimental data taken from the literature[11] is also included for comparison. In general, computer simulation is able to predict very accurately the vapour and liquid densities in the whole range of temperatures considered, from near the triple-point to the critical temperature. Very small differences between simulation and experimental data for the liquid branch of the phase envelope can be seen at low temperatures in the case of methyl acetate, methyl propionate, and methyl butyrate.

In addition to the vapour and liquid coexistence densities, we have also determined the coordinates of the critical points of all the FAMEs for the MD simulation results using the scaling laws given by Eqs. (3) and (4). In particular, we follow the methodology explained in the previous section. As in the case of the vapour and liquid coexistence densities, we compare our results obtained from the analysis described above with experimental data taken from the literature[11]. The critical temperatures and densities of all the FAMEs obtained from MD simulations are presented in Table 6. Comparison between simulation and experimental critical coordinates can also be observed in Fig. 2. Agreement between simulation and experiments is excellent in all cases. Computer simulation results overestimate the experimental values less than a 3% (2.7% is the case of methyl hexanoate and 0.7% in the case of methyl butyrate). Differences between experiment and simulation could be due to finite-size scaling effects that occur during simulations when the system is close to the critical state. These effects can be taken into account explicitly using advanced simulation techniques, such as the Finite-Size Scaling procedure of Binder[48]. However, this kind of analysis is out of the scope of this work. Critical densities of the homologous chemical family is also accurately predicted by the TraPPE-UA models of FAMEs. Deviation between simulation and experiments for ρ_c is always below 2%, except in the case of methyl valerate (5.9%). In all cases, critical densities are slightly overestimated as expected.

We have also determined the normal boiling temperature of each methyl ester. This has been done using Eq. (6) and evaluating the pressure at $P = 101325$ Pa. Predictions from simulation are shown in Table 6. Comparison between values taken from the literature and prediction obtained from simulation show a good agreement between both results. As can be seen, in most cases the deviation is $\approx 2.2-3.8\%$, except in the case of methyl hexanoate, in which deviation is 4.69%, approximately.

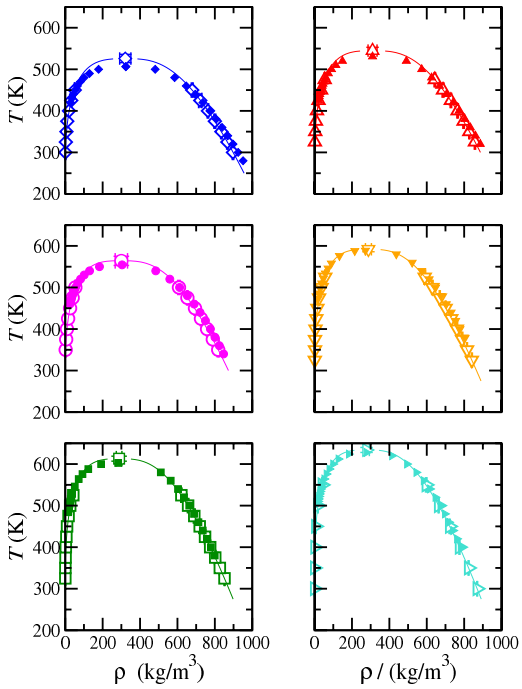

Fig. 2 Vapour-liquid coexistence densities of methyl esters. The open symbols correspond to the coexistence densities obtained from MD NVT simulations and the filled symbols to the experimental data taken from the literature[11] for methyl acetate (blue diamonds), methyl propionate (red triangles up), methyl butyrate (magenta circles), methyl pentanoate (orange triangles down), methyl hexanoate (green squares), and methyl heptanoate (turquoise triangles right). The continuous curves correspond to the fits of the simulation data presented in this work to Eqs. (3) and (4). Symbols at the highest temperatures for each coexistence curve represent the critical points estimated from Eqs. (3) and (4) (filled symbols) and the experimental critical points taken from the literature[11] (open symbols).

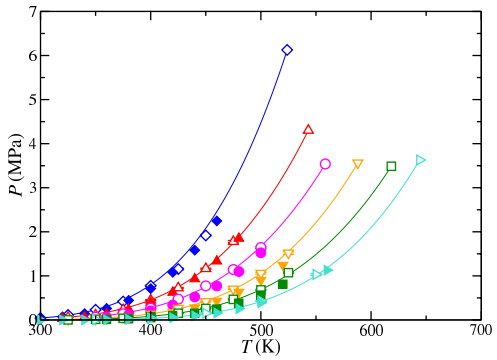

Fig. 3 Vapour pressure of methyl esters (from methyl acetate to methyl heptanoate). The meaning of the symbols is the same as in Fig. 2. The continuous curves correspond to the fits of the simulation data presented in this work to Eq. (6). Filled symbols at the highest temperature for each vapour pressure curve represent the critical points obtained from Eq. (6) using the critical temperature values obtained from Eq. (3).

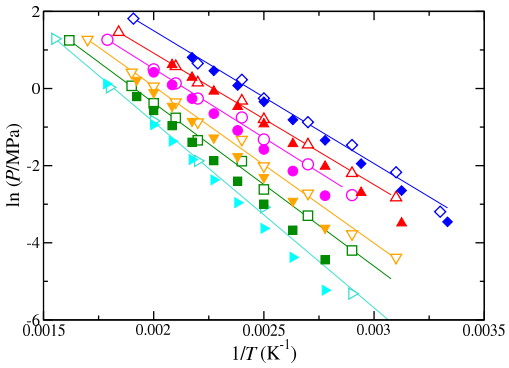

Fig. 4 Clausius-Clapeyron representation of the vapour pressure of methyl esters (from methyl acetate to methyl heptanoate). The meaning of the symbols is the same as in Fig. 2.

Vapour pressure of FAMEs is also calculated from MD simulation. Since we are simulating planar vapour-liquid interfaces, the system is inhomogeneous. Consequently, the pressure is no longer a scalar magnitude but a tensorial quantity. In this case, the normal component of the pressure tensor (acting perpendicularly to the planar interface) is equal to the vapour pressure of the system. The results obtained from computer simulations are shown in Table 5. We have also presented the vapour pressure, as functions of temperature, of all the FAMEs studied in this work in Figure 3. Prediction obtained from computer simulations provide, in general, a good description of the vapour pressure curves, particularly for methyl acetate, methyl propionate, and methyl heptanoate. As can be seen in Figure 3, in the case of methyl butyrate, methyl valerate, and methyl hexanoate, MD simulation results overestimate the vapour pressure at mid and high temperatures. We have also represented the vapour pressure data in a Clausius-Clapeyron plot (Figure 4). TraPPE-UA models are able to predict very accurately the vapour pressure of all the FAMEs, from methyl acetate up to methyl heptanoate, at low temperatures.

One of the main goals of this work is to predict the interfacial properties of FAMEs. Figure 5 displays the variation of the interfacial thickness, d, as a function of temperature obtained using Eq. (9) for each FAME. From this Figure it is possible to observe that d increases with increasing temperature. This means that the interfacial region becomes wider as the temperature is increased. At low temperatures, the density profiles show sharp interfaces, which can be identified with low values of interfacial thickness. An increase of the temperature results in a wider interfacial region as the system approaches the critical point, and consequently, the interfacial thickness increases. As $T \to T_c$, the interfacial thickness diverges as the liquid and vapour phases become identical.

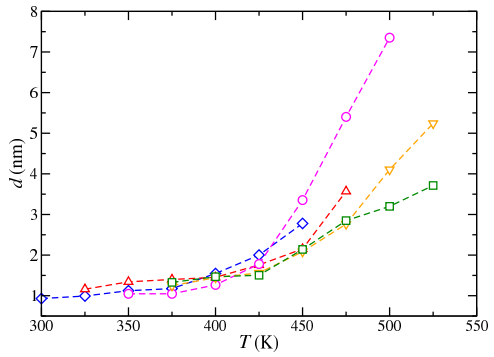

Fig. 5 10-90 interfacial thickness d as a function of the temperature for methyl esters (from methyl acetate to methyl heptanoate). The symbols correspond to the values obtained from density profiles obtained from MD NVT simulations and the dashed curves are included as a guide to the eye. The meaning of the symbols is the same as in Fig. 2.

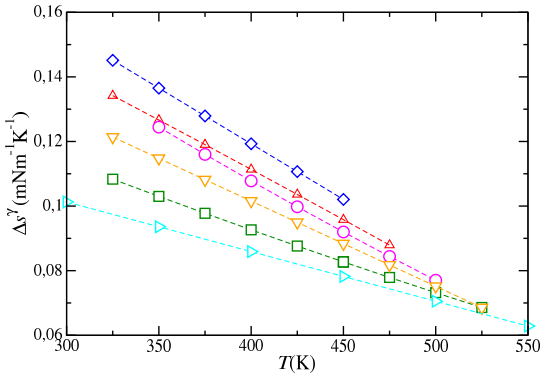

Fig. 6 Surface entropy of methyl esters (from methyl acetate to methyl heptanoate) as obtained from the combination of the MD NVT simulation results and Eq. (7). The meaning of the symbols is the same as in Fig. 2.

The surface entropy, Δs^γ, that can obtained from the temperature derivative of the surface tension according to Eq. (7), is an useful magnitude in studies involving surfaces in which temperature, and also surface tension, is non-uniform, leading to the well-known Bénard-Marangoni convection phenomena[49]. Fig. 6 shows the surface entropy change of surface formation for FAMEs as a function of temperature. Δs^γ is obtained from MD computer simulations of the interfacial tension in combination with Eq. (7). Δs^γ varies linearly with T for all the methyl esters considered here and slightly decreases with increasing temperature. This behaviour is related with the slight curvature of the surface tension as a function of temperature (see below). In addition to that, for a fixed temperature, Δs^γ exhibits its largest values for short methyl esters and gets smaller as the molecular weight of the FAME increases. This indicates that curvature of surface tension, as a function of temperature, is larger for short methyl esters than for long FAMEs. Interestingly, as the temperature increases, differences between Δs^γ for FAMEs becomes smaller, showing that curvature of surface tension, at high temperature, is similar for all methyl esters. This is a clear indication of the universal behaviour of $\gamma = \gamma(T)$ for different members of the homologous series as the system approaches the critical region.

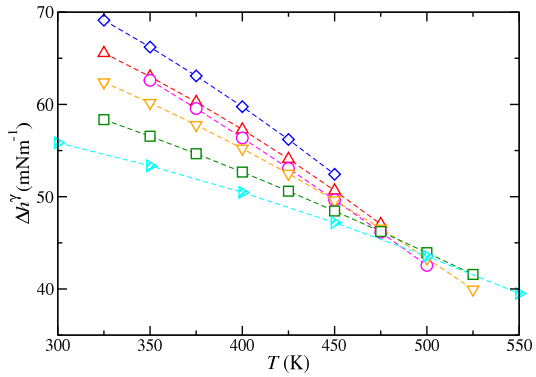

Fig. 7 Surface enthalpy of methyl esters (from methyl acetate to methyl heptanoate) as obtained from the combination of the MD NVT simulation results and Eq. (8). The meaning of the symbols is the same as in Fig. 2.

It is possible to obtain the surface enthalpy, Δh^γ, as a function of temperature, for the FAMEs studied in this work. As in the case of the surface entropy, Δh^γ can be determined from MD simulation data of the interfacial tension using Eq. (8). According to this, surface enthalpy is computed directly from surface tension values and the numerical derivative of $\gamma(T)$ with respect to the temperature. Fig. 7 shows Δh^γ, as a function of temperature, of the methyl esters. As can be seen, this property decreases with temperature, as expected. A nearly linear behaviour is observed for the shortest FAMEs. However, the $\Delta h^\gamma - T$ plots show a certain curvature as the molecular weight is increased. At fixed temperature, the surface enthalpy decreases as the lengths of the methyl esters are increased. Although this is true at low and mid temperatures, this trend seems to change as T is high.

Finally, we consider the vapour-liquid interfacial tension of methyl esters, from methyl acetate up to methyl heptanoate. Fig. 8 shows the surface tension, as a function of temperature, as obtained from MD simulations using the virial or mechanical route. According to this, the surface tension is calculated using Eq. (2), i.e., as the difference between the normal and tangential macroscopic components of the pressure tensor. We have also included experimental data taken from the literature[11] in order to compare the predictions from the TraPPE-UA molecular models. Simulation results obtained in this work show an excellent agreement with experimental data in the temperature range at which experimental data is available ($T \lesssim 360$ K). Simulation results obtained from the use of TraPPE-UA models for methyl esters seem to slightly overestimate the surface tension at low temperatures for methyl acetate, methyl propionate, and methyl butyrate. For longer molecules, agreement between simulation and experimen-

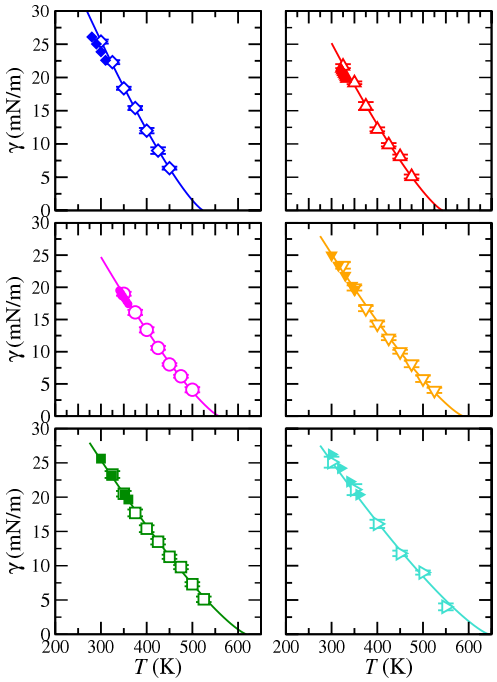

Fig. 8 Vapour-liquid surface tension as function of temperature for methyl esters (from methyl acetate to methyl heptanoate). The meaning of the symbols is the same as in Fig. 2. The continuous curves correspond to the fits of the simulation data presented in this work to Eq. (5).

tal data is excellent.

As in the case of the vapour-liquid phase envelopes, we have also fit the simulation data using the well-known Guggenheim's scaling law for the surface tension as a function of temperature according to Eq. (5)[38,39]. This allows to obtain the critical temperature of each methyl ester and compare these values with the experimental critical values. Table 6 includes the values found in this work. It is interesting to compare the critical values obtained from Eqs. (3)-(4) and (5). As can be seen, critical temperatures determined using surface tension values and vapor and liquid coexistence densities are different. A priori, one expects that both values should be the same. However, one should take into account the following points: (1) Strictly speaking, the scaling laws given by Eqs. (3) and (5) are only valid in the asymptotic limit $T \to T_c$; in this work, as it is usual in the literature[41,42,44,50,51], we have used data corresponding to states located at T far away from T_c (data corresponding to temperatures from around a $30-40\%$ below the critical temperature up to near the critical point). (2) The estimation of the critical coordinates depends critically on the size of the system; here we use only 1100 molecules, which in our opinion, it is not enough to avoid the finite-size effects of the systems under study[52]. (3) The location of the critical coordinates depends also critically on the cutoff distance used during the simulation, and if tail corrections are applied or not. This is especially important if we are using two different kind of properties (density and surface tension values) to obtain the critical temperature since they are affected by the truncation of the intermolecular potential in a different way, as it probably happens in this work. (4) Finally, the goal of the this work is not to obtain accurate values of critical temperatures and densities of methyl esters but to check if TraPPE force field is able to predict, in a transferable manner, the phase equilibria and interfacial properties of methyl esters. We think a procedure similar to that followed by Dinpajooh *et al.*[52], finite-size scaling[53] or mixed-field theory using the Binder cumulant parameter[54] methodologies, is the correct approach to be followed if accurate estimations of critical points are needed. Unfortunately, this is out of the scope of this work.

It is interesting to mention that experimental data taken from the literature[11] is only available at low temperatures, from 300 up to 360 K, approximately. The reason for which there is no experimental data at higher temperatures is that methyl esters become unstable as temperature is higher, generating micro bubbles in the tensiometer and densimeter, making impossible to measure this property accurately. Fortunately, this is not the case for computer simulations. Our study allows to obtain the surface tension of all the methyl esters analyzed in this work up to $450-550$ K, depending on the critical temperature of each substance. It is important to recall that the simulated surface tension values in this work are, to the best of our knowledge, reported for the first time. This is particularly important in this case since there is none experimental data at temperatures above 360 K for non of the FAMEs studied, as just commented. The excellent agreement found, not only for surface tension at low temperatures, but also for vapour-liquid coexistence densities and vapour pressures in wide ranges of temperatures, makes the TraPPE-UA models proposed and used in this work excellent candidates for predicting the phase equilibria and interfacial properties of FAMEs. Simulation data presented in this work could be used, not only for theoretical modelling of these compounds, but also for the design and use of new chemical processes involving FAMEs as future and alternative diesel fuels, as well as for environmental issues, including the removal of contaminants from water and for groundwater remediation.

5 Conclusion

We have studied the phase equilibria and interfacial properties of methyl esters homologous series (from methyl acetate to methyl heptanoate) using the TraPPE force fields for different molecules and chemical families in a transferable way. In particular, we use the direct coexistence technique, in combination with MD NVT simulations, to study inhomogeneous systems of pure esters containing two vapour-liquid interfaces.

We examine the vapour-liquid surface tension using the virial route, i.e., calculating the normal and tangential components of the pressure tensor. We have also determined density profiles, coexistence densities, vapour pressures, surface entropies and enthalpies, interfacial thickness, and critical temperature, density, and pressure as functions of temperature for all the methyl esters

considered. Predictions from the MD simulation for vapour-liquid coexistence densities and vapour pressures are compared with experimental data taken from the literature. These three properties are predicted remarkably well by the TraPPE models. This is particularly important since the molecular parameters of the TraPPE force fields are taken in a transferable way from other molecules and chemical families without need of adjustment.

We also predict the behaviour of interfacial thickness, surface entropy, and surface enthalpy, as functions of temperatures, and consider the effect of increasing the molecular weight of the homologous family. Particularly interesting are the results for the surface tension of methyl esters. The TraPPE models and the molecular parameters transferred from other molecules and chemical families are able to predict very accurately the surface tension of all the methyl esters studied in this work at low temperatures. Although experimental data is only available at temperatures below 360 K, computer simulations allows us to provide surface tension up to the pure critical points of each substance. This is an important result since this is the first time the vapour-liquid surface tension of methyl esters is determined in the literature at these conditions. In fact, this is the first computer simulation work devoted to the prediction of the vapour-liquid equilibria and interfacial properties of the homologous series.

6 Acknowledgement

The authors acknowledge Centro de Supercomputación de Galicia (CESGA, Santiago de Compostela, Spain) for providing access to computing facilities, and Ministerio de Economía, Industria y Competitividad through Grant with reference FIS2017-89361-C3-1-P co-financed by EU FEDER funds. A.M. acknowledges funding from Fondecyt (Chile) through Grant 1190107. Further financial support from Junta de Andalucía and Universidad de Huelva is also acknowledged. J.A.F. acknowledges Contrato Predoctoral de Investigación from XIX Plan Propio de Investigación de la Universidad de Huelva and a FPU Grant (Ref. FPU15/03754) from Ministerio de Educación, Cultura y Deporte. J.A., J.M.M., P.G.-A., and F.J.B. thankfully acknowledge the computer resources at Magerit and the technical support provided by the Spanish Supercomputing Network (RES) (Project QCM-2018-2-0042).

References

1 *https://ec.europa.eu/energy/en/topics/renewable-energy/renewable-energy-directive, (retrieved November, 2019)*.

2 M. Faith Demirbar, *Applied Energy*, 2009, **86**, S151–S161.

3 L. C. B. A. Bessa, M. C. Ferreira, C. R. A. Abreu, E. A. C. Batista and A. J. A. Meirelles, *Fluid Phase Equil.*, 2016, **425**, 98–107.

4 N. D. D. Carareto, M. C. Costa, A. J. A. Meirelles and J. Pauly, *Fluid Phase Equil.*, 2014, **382**, 158–163.

5 N. D. D. Carareto, C. Y. C. S. Kimura, E. C. Oliveira, M. C. Costa and A. J. A. Meirelles, *Fuel*, 2012, **96**, 319–326.

6 *DECHEMA Gesellschaft Für Chemische Technik Und Biotechnologie E.V., Frankfurt Am Main, Germany, https://i-systems.dechema.de/detherm/, (retrieved November, 2019)*.

7 C. Wohlfarth and B. Wohlfarth, *New Series Group IV Physical Chemistry*, Springer Verlag, Berlin, Heidelberg, 1997, vol. 16.

8 C. Wohlfarth and B. Wohlfarth, *New Series Group IV Physical Chemistry*, Springer Verlag, Berlin, Heidelberg, 2008, vol. 24.

9 C. Wohlfarth and B. Wohlfarth, *New Series Group IV Physical Chemistry*, Springer Verlag, Berlin, Heidelberg, 2016, vol. 28.

10 T. E. Daubert and R. P. Danner, *Physical and Thermodynamic Properties of Pure Chemicals. Data Compilation*, Taylor and Francis, Bristol, 1989.

11 E. W. Lemmon, M. O. McLinden, D. G. Friend, C. Wohlfarth and B. Wohlfarth, *NIST Chemistry WebBook, NIST Standard Reference Database Number 69*, National Institute of Standards and Technology: Gaithersburg MD, 2019.

12 H. T. Davies and L. E. Scriven, *Adv. Chem. Phys.*, 1982, **49**, 357.

13 I. del Pozo, M. Cartes, F. Llovell and A. Mejía, *J. Chem. Thermodynamics*, 2018, **121**, 121–128.

14 T. J. Bruno, T. M. Loestead, J. R. Riggs, E. L. Jorgenson and M. L. Huber, *Energy Fuels*, 2011, **25**, 2493–2507.

15 J. E. Landmeyer, P. M. Bradley, D. A. Trego, K. G. Hale and J. E. Haas, *Ground Water*, 2010, **48**, 30–41.

16 *http://chem-siepmann.oit.umn.edu/siepmann/trappe/index.html, (retrieved November, 2019)*.

17 G. Kamath, J. Robinson and J. J. Potoff, *Fluid Phase Equil.*, 2006, **240**, 46–55.

18 J. J. Potoff and J. I. Siepmann, *AIChE Journal.*, 2001, **47**, 1676–1682.

19 G. Kamath, F. Cao and J. J. Potoff, *J. Phys. Chem. B*, 2004, **108**, 14130–14136.

20 J. Stubbs, J. J. Potoff and J. I. Siepmann, *J. Phys. Chem. B*, 2004, **108**, 17596–17605.

21 G. M. Martin and J. I. Siepmann, *J. Phys. Chem. B*, 2001, **102**, 2569–2577.

22 K. A. Maerzke, N. E. Schultz, R. B. Ross and J. I. Siepmann, *J. Phys. Chem. B*, 2009, **113**, 6415–6425.

23 D. Frenkel and B. Smit, *Understanding Molecular Simulations*, 2nd Ed. Academic, San Diego, 2002.

24 M. P. Allen and D. J. Tildesley, *Computer Simulation of Liquids, 2 Ed.*, Oxford University PressClaredon, Oxford, 2017.

25 D. van der Spoel, E. Lindahl, B. Hess, G. Groenhof, A. E. Mark and H. J. Berendsen, *J. Comput. Chem.*, 2005, **26**, 1701–1718.

26 G. Galliero, M. M. Piñeiro, B. Mendiboure, C. Miqueu, T. Lafitte and D. Bessieres, *J. Chem. Phys.*, 2009, **130**, 104704/1–10.

27 G. Galliero, *J. Chem. Phys.*, 2010, **133**, 074705/1–7.

28 J. M. Míguez, M. M. Piñeiro and F. J. Blas, *J. Chem. Phys.*, 2013, **138**, 034707/1–11.

29 M. A. Cuendet and W. F. V. Gunsteren, *J. Chem. Phys.*, 2007, **127**, 184102/1–9.

30 S. Nosé, *Mol. Phys.*, 1984, **52**, 255–268.

31 H. J. C. Berendsen, J. P. M. Postma, W. F. V. Gunsteren, A. D. Nola and J. R. Haak, *J. Chem. Phys.*, 1984, **81**, 3684/1–8.

32 H. Hulshof, *Ann. Phys. (Berlin)*, 1901, **4**, 165–186.

33 J. S. Rowlinson and B. Widom, *Molecular Theory of Capillarity*, Claredon Press, 1982.

34 E. D. Miguel, F. J. Blas and E. M. D. Río, *Mol. Phys.*, 2006, **104**, 2919–2927.

35 E. D. Miguel and G. Jackson, *J. Chem. Phys.*, 2006, **125**, 164109/1–12.

36 J. S. Rowlinson and F. L. Swinton, *Liquids and Liquid Mixtures*, Butterworth, London, 1982.

37 H. W. Xiang, *The Corresponding-States Principle and Its Practice Thermodynamic. Transport and Surface Properties of Fluids*, Elsevier, Amsterdam, 2005.

38 E. A. Guggenheim, *J. Chem. Phys.*, 1945, **13**, 253–261.

39 B. Widom, *J. Chem. Phys.*, 1965, **43**, 3892.

40 M. Modell and J. D. Tester, *Thermodynamics and its applications, thrid edition*, iPrentice-Hall, New York, 1998.

41 F. J. Blas, L. G. MacDowell, E. D. Miguel and G. Jackson, *J. Chem. Phys.*, 2008, **129**, 144703.

42 L. G. MacDowell and F. J. Blas, *J. Chem. Phys.*, 2009, **131**, 074705/1–10.

43 J. G. Sampayo, F. J. Blas, E. D. Miguel, E. A. Müller and G. Jackson, *J. Chem. Eng. Data*, 2010, **55**, 4306.

44 F. J. Blas, A. I. Moreno-Ventas Bravo, J. M. Míguez, M. M. Piñeiro and L. G. MacDowell, *J. Chem. Phys.*, 2012, **137**, 084706.

45 J. M. Garrido, M. Cartes, A. Mejía, J. Algaba, J. M. Míguez, F. J. Blas, A. I. Moreno-Ventas Bravo and M. M. Piñeiro, *J. Supercrit. Fluids*, 2017, **128**, 359–369.

46 J. Algaba, J. M. Garrido, J. M. Míguez, A. Mejía, A. I. M.-V. Bravo and F. J. Blas, *J. Phys. Chem. C*, 2018, **122**, 16142–16153.

47 J. Algaba, M. Cartes, A. Mejía, J. M. Míguez and F. J. Blas, *J. Phys. Chem. C*, 2019, **123**, 20960–20970.

48 K. Binder, *Z. Phys. B Condensed Matter*, 1981, **43**, 119.

49 E. Salomon and M. Mareschal, *J. Phys.: Condens. Matter*, 1991, **3**, 3645.

50 F. J. Blas, A. I. Moreno-Ventas Bravo, J. A. Fernández, F. J. Martínez-Ruiz and L. G. MacDowell, *J. Chem. Phys.*, 2014, **140**, 114705/1–114705/11.

51 F. J. Martínez-Ruiz, F. J. Blas, B. Mendiboure and A. I. Moreno-Ventas Bravo, *J. Chem. Phys.*, 2014, **141**, 184701.

52 M. Dinpajooh, P. Bai, D. A. Allan and J. I. Siepmann, *J. Chem. Phys.*, 2015, **143**, 114113–1–114113–13.

53 J. J. Potoff and T. Z. Panagiotopoulos, *J. Chem. Phys.*, 1998, **109**, 10914–10920.

54 J. Pérez-Pellitero, P. Ungerer, G. Orkoulas and A. D. Mackie, *J. Chem. Phys.*, 2006, **125**, 054515–1–054515–9.

Table 5 Liquid density ρ_L, vapour density ρ_V, vapour pressure P, compressibility factor Z, and surface tension γ at different temperatures, as obtained from MD NVT simulations for methyl esters (from methyl acetate to methyl heptanoate). The errors are estimated as explained in the text.

T(K)	ρ_L(kg/m^3)	ρ_V(kg/m^3)	P(MPa)	Z	γ(mN/m)
			Methyl acetate		
300	897(3)	1.2(1)	0.041(3)	1.06 (1)	-
325	867(3)	3.3(2)	0.114(7)	0.946(2)	22.3(3)
350	835(3)	6.5(3)	0.231(8)	0.90(1)	18.4(2)
375	800(4)	10.7(5)	0.42(1)	0.93(2)	15.4(3)
400	763(3)	20.0(6)	0.78(1)	0.86(1)	12.0(4)
425	722(8)	32.0(7)	1.26(2)	0.821(7)	9.0(5)
450	679(4)	51(1)	1.92(1)	0.75(1)	6.4(2)
			Methyl propionate		
325	858(2)	1.8(2)	0.06(3)	1.07(4)	21.7(3)
350	828(2)	3.6(2)	0.111(4)	0.94(2)	19.2(2)
375	797(3)	7.2(0.4)	0.233(9)	0.91(2)	15.7(6)
400	765(3)	12.8(5)	0.45(1)	0.93(2)	12.2(3)
425	729(3)	21.1(6)	0.726(9)	0.86(1)	9.9(3)
450	687(4)	34.7(7)	1.16(1)	0.788(8)	8.1(3)
475	643(3)	54(1)	1.78(3)	0.733(3)	5.1(3)
			Methyl butyrate		
350	818(4)	2.0(3)	0.063(5)	1.10(8)	19.0(3)
375	790(2)	4.8(3)	0.140(6)	0.95(2)	16.1(4)
400	759(3)	8.9(5)	0.267(5)	0.92(3)	13.4(4)
425	726(3)	15.3(5)	0.472(8)	0.89(1)	10.6(3)
450	694(4)	26(1)	0.77(1)	0.81(1)	8.0(2)
475	653(3)	39.3(1)	1.14(2)	0.751(8)	6.2(2)
500	608(5)	54(2)	1.64(2)	0.75(8)	4.1(4)
			Methyl valerate		
375	789(3)	2.5(3)	0.066(5)	0.98(4)	16.7(4)
400	761(3)	5.1(4)	0.134(6)	0.92(3)	14.3(4)
425	731(2)	9.4(3)	0.27(1)	0.928(9)	12.1(3)
450	701(2)	15.1(6)	0.42(1)	0.858(9)	10.0(3)
475	670(2)	24.0(5)	0.70(1)	0.860(6)	8.1(5)
500	630(3)	37.8(1)	1.06(2)	0.782(8)	5.8(5)
525	589(4)	56.9(2)	1.52(3)	0.710(5)	4.0(4)
			Methyl hexanoate		
375	802(3)	1.7(2)	0.037(4)	0.92(3)	17.7(5)
400	775(2)	2.9(2)	0.073(5)	0.984(4)	15.4(5)
425	748(2)	5.9(3)	0.152(6)	0.95(1)	13.5(4)
450	719(4)	9.7(5)	0.26(1)	0.935(9)	11.3(3)
475	690(4)	17.6(5)	0.47(1)	0.873(2)	9.8(3)
500	657(3)	26.5(8)	0.68(1)	0.80(1)	7.3(3)
525	621(2)	43(1)	1.07(2)	0.742(7)	5.1(4)
			Methyl heptanoate		
300	870(2)	0.02(1)	-	-	25.1(8)
350	824(2)	0.36(4)	-	-	21.1(8)
400	775(2)	2.2(2)	0.046(5)	0.993(4)	16.1(6)
450	722(2)	6.1(4)	0.15(1)	1.06(1)	11.8(4)
500	663(2)	17.4(6)	0.43(1)	0.944(9)	9.0(3)
550	597(3)	41(1)	1.03(2)	0.869(8)	4.0(5)

Table 6 Experimental (T_c^{exp}, ρ_c^{exp}, P_c^{exp}, and T_b^{exp}) and predicted ($T_c^\dagger$, $T_c^\S$, $\rho_c^\dagger$, $P_c^\dagger$, and T_b) critical temperatures, densities, and pressures and normal boiling temperatures of methyl esters (from methyl acetate to methyl heptanoate). Critical temperatures, $T_c^\dagger$ and $T_c^\S$, are obtained from the analysis of the MD NVT coexistence densities using Eqs. (3) and (4), and the analysis of the MD NVT tension data using Eq. (5), respectively. Critical densities, $\rho_c^\dagger$, are also obtained from the analysis of the MD NVT coexistence densities using Eq. (4). Critical pressures, $P_c^\dagger$, are obtained using Eq. (6) evaluating the temperature $T_c^\dagger$ as obtained from Eq. (3). Normal boiling temperatures are obtained using Eq. (6) evaluating the pressure at $P = 101325$ Pa.

Substance	T_c^{exp}(K)	$T_c^\dagger$(K)	$T_c^\S$(K)	ρ_c^{exp}(kg/m^3)	$\rho_c^\dagger$(kg/m^3)	P_c^{exp}(MPa)	$P_c^\dagger$(MPa)	P_b^{exp}(MPa)	P_b(MPa)
Methyl acetate	510.0	523.9	525.14	324.0	321.0	4.692	6.127	322.63	330.09
Methyl propionate	531.5	543.1	550.38	310.0	310.0	3.986	4.302	340.10	352.44
Methyl butyrate	554.5	558.8	571.65	304.0	300.0	3.464	3.538	359.35	373.60
Methyl valerate	566.9	558.0	589.80	272.0	288.0	3.090	3.564	388.09	400.65
Methyl hexanoate	602.6	618.4	597.46	283.0	288.0	2.797	3.487	407.72	427.81
Methyl heptanoate	628.0	644.1	635.28	278.0	278.0	2.543	3.630	435.71	446.15